Chem Soc Rev

Focusing on a nickel hydrocorphinoid in a protein matrix: Methane generation by methyl-coenzyme M reductase with F430 cofactor and its models

Journal:	*Chemical Society Reviews*
Manuscript ID	CS-REV-09-2021-000840.R1
Article Type:	Review Article
Date Submitted by the Author:	30-Dec-2021
Complete List of Authors:	Miyazaki, Yuta; Osaka University, Applied Chemistry Oohora, Koji; Osaka University, Applied Chemistry Hayashi, Takashi; Osaka University, Applied Chemistry

ARTICLE

Focusing on a nickel hydrocorphinoid in a protein matrix: Methane generation by methyl-coenzyme M reductase with F430 cofactor and its models

Received 00th January 20xx,
Accepted 00th January 20xx

DOI: 10.1039/x0xx00000x

Yuta Miyazaki,[a,†] Koji Oohora[a,*] and Takashi Hayashi[a,*]

Methyl-coenzyme M reductase (MCR) containing a nickel hydrocorphinoid cofactor, F430, is an essential enzyme which catalyze anaerobic methane generation and oxidation. The active Ni(I) species in MCR converts methyl-coenzyme M (CH_3S–CoM) and coenzyme B (HS–CoB) to methane and heterodisulfide (CoM–S–S–CoB). Extensive experimental and theoretical studies focusing on the substrate-binding cavity including the F430 cofactor in MCR have suggested two principally different reaction mechanisms involving an organonickel CH_3–Ni(III) species or a transient methyl radical species. In parallel with research on native MCR itself, the functionality of MCR has been investigated in context of model complexes of F430 and recent protein-based functional models which include a nickel complex. In the latter case, hemoproteins reconstituted with tetradehydro- and didehydrocorrinoid nickel complexes have been found to represent useful model systems responsible for methane generation. These efforts support the proposed mechanism of the enzymatic reaction and provide important insights into replicating the MCR-like methane generation process. Furthermore, the modeling of MCR described here is expected to lead to understanding of protein-supported nickel porphyrinoid chemistry as well as the creation of MCR-inspired catalysis.

Introduction

Macrocyclic tetrapyrrole derivatives are quite common in nature. One of the typical natural tetrapyrrole compounds is porphyrin, which commonly acts as a dianionic ligand, binding an iron ion to form the natural compound known as heme, a versatile cofactor (prosthetic group) with an aromaticity of 18 π electrons. Many hemoproteins include the *b*-type heme cofactor based on protoporphyrin IX, the simplest porphyrin (Fig. 1a). These hemoproteins porvide various functions such as oxygen storage/transfer, oxidation/oxygenation, and electron transfer, among others.[1] Chlorophylls are another class of versatile metal cofactors which contain Mg^{2+} as a central metal ion bound to a partially hydrogenated and substituted porphyrin ligand (Fig. 1b). It is a key cofactor in the photosynthetic center of plants.[2] Another example of a distinct macrocyclic cofactor is the well-known cobalt tetrapyrrole complex known as cobalamin, which is formed by a corrin ring lacking one meso position in the macrocycle relative to porphyrin. This macrocyle acts as a monoanionic ligand (Fig. 1c), and the organocobalt species is employed as an intermediate of cobalamin-dependent catalysis.[3] Another class of porphyrinoid cofactor, F430, was discovered in methane-producing microorganisms in 1978.[4] The F430 cofactor is a nickel complex with a highly hydrogenated and monoanionic porphyrinoid known as hydrocorphin (Fig. 1d).[5] The nickel cofactor is responsible for methane generation in methyl-coenzyme M reductase (MCR) from *Archaea* (*vide infra*).[6] MCR and F430 are not as well characterized as hemoproteins and cobalamin-dependent proteins. This review briefly outlines the structure and function of MCR and describes model studies focusing on the replication of the unique F430 cofactor in efforts to understand its physicochemical properties and reactivities.

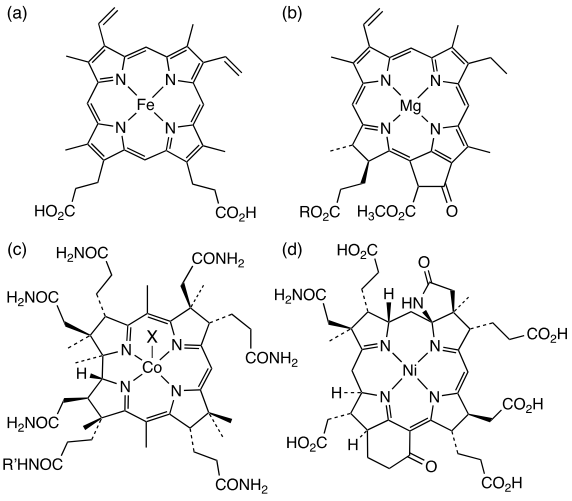

a. Department of Applied Chemistry, Graduate School of Engineering, Osaka University, Suita 565-0871, Japan. E-mail: thayashi@chem.eng.osaka-u.ac.jp
† Present address: JSR Corporation, Tsukuba 305-0841, Japan.

Fig. 1. Structure of representative naturally-occurring metalloporphyrinoids. (a) heme *b*, (b) chlorophyll *a* where R represents a side chain consisting of a hydrocarbon tail, (c) cobalamin where R' represents a side chain containing of a benzimidazole ligand and an adenosyl moiety, (d) F430.

1. Methanogenesis

Methane generation and oxidation under anaerobic conditions are biochemical reactions of anaerobic microbes, especially methanogens. Methanogens such as *Methanosarcina* produce methane from representative carbon sources such as H_2/CO_2, methylated compounds, acetate, and methanol, whereas others such as *Methanobacterium* can only utilize H_2/CO_2.[7] Fig. 2a shows the last two steps of energy metabolism in methanogenic bacteria, in which methyl-coenzyme M (methyl-mercaptoethanesulfonate, $CH_3S{-}CoM$) is produced from CO_2 in the first six steps and reduced to methane by MCR. This is an essential enzyme catalyzing the reaction in the final and rate-determining step of methane generation in a series of enzymes responsible for carbon source transformation. Other carbon sources are also converted to methyl-coenzyme M in different metabolic pathways in methanogens and subsequently reduced to methane by MCR as in the case using CO_2/H_2, regardless of the origin of required energy and carbon source. Furthermore, it has been recently discovered that MCR is included in the first step of anaerobic methane oxidation by anaerobic methanotrophic archaea (ANMEs) and the reaction is expected to proceed as part of the reverse mechanism of methane generation by methanogens.[8,9] MCR also appears to be involved in the anaerobic oxidation of short chain alkanes, such as ethane, propane, and butane, to CO_2 via the formation of corresponding alkyl-coenzyme M ((alkyl)S−CoM) derivatives.[10,11]

1.1 Methyl-coenzyme M reductase (MCR)

MCR is a key enzyme for biological methane generation and oxidation under anaerobic conditions.[12-14] The reaction mechanism of MCR in anaerobic methane generation has been extensively investigated since the identification of MCR from cell extracts of *Methanothermobacter thermoautotrophicus* in the 1980s by Wolfe and coworkers.[15] Relative to methane generation, involvement of MCR in anaerobic methane oxidation has been investigated since 2003 when MCR was isolated from microbial mats which anaerobically oxidize methane.[8] MCR which includes nickel hydrocorphin F430 as a cofactor, catalyzes the exergonic reaction ($\Delta G°$ = −30 kJ·mol^{-1}) of $CH_3S{-}CoM$ with coenzyme B (*N*-7-mercaptoheptanoylthreonine phosphate, HS−CoB) to produce methane and the mixed heterodisulfide (CoM−S−S−CoB) under strictly anaerobic conditions (Fig. 2bc). The coenzymes, $CH_3S{-}CoM$ and HS−CoB, are known to work as a methyl group donor and an electron donor, respectively. It was very difficult to isolate the active MCR from methanogens because MCR is extremely oxygen-sensitive. Thauer and coworkers first purified MCR and reproduced the active state by the reduction of an inactivated state using Ti(III) citrate under alkaline conditions in the 1990s.[16,17]

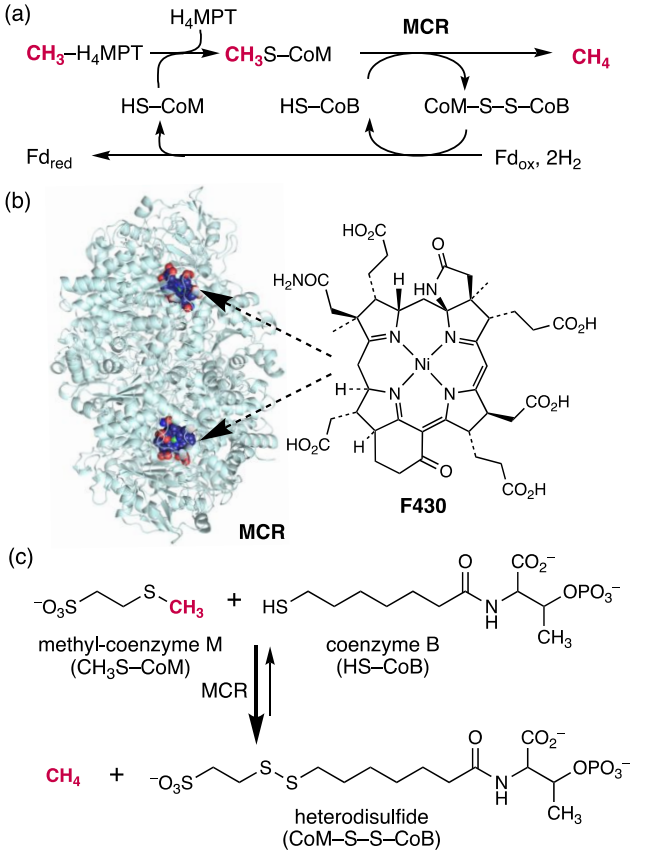

Fig. 2. (a) Reaction scheme of the last two steps in energy metabolism of methanogenic bacteria for methane generation from CO_2 and H_2. H_4MPT: tetrahydromethanopterin, HS–CoM: coenzyme M, Fd: ferredoxin. (b) Crystal structure of MCR from *Methanobacterium thermoautotrophicum* (PDB ID: 1MRO). (c) Methane generation catalyzed by MCR.

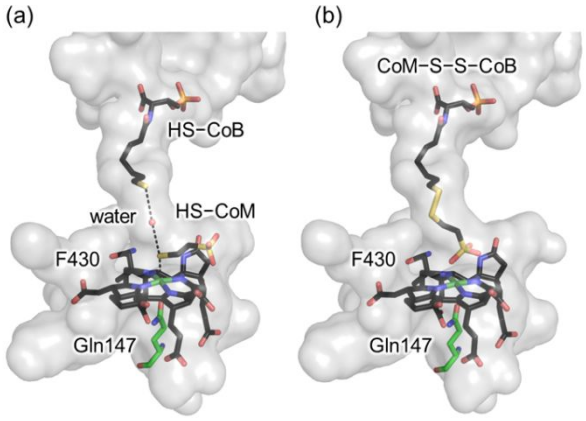

Fig. 3. The active site and substrate channel shown in gray surfaces in the crystal structure of (a) $MCR_{ox1\text{-}silent}$ (PDB ID: 1HBN) and (b) MCR_{silent} (PDB ID: 1HBM).

The first crystal structure of MCR with 1.45 Å resolution was obtained from *M. marburgensis* containing an inactivated state of MCR, $MCR_{ox1\text{-}silent}$, by Thauer and coworkers.[18] It was found that MCR is composed of three different subunits, McrA (ca. 65

kDa), McrB (ca. 45 kDa), and McrG (ca. 35 kDa), in an $(\alpha\beta\gamma)_2$ heterohexamer containing two sets of active sites containing the F430 cofactor and funnel-shaped substrate-binding channel constructed with nonpolar and aromatic amino acid residues, such as Phe and Tyr. F430 is buried at the bottom of the substrate-binding channel as the inactive Ni(II) state and coordinated by the oxygen atom of the side chain of Gln147 and the thiol moiety of HS−CoM in the proximal and distal sides of the hydrophobic active site, respectively. HS−CoM fits into the active site with interactions including a salt bridge and hydrogen bonding interactions of its sulfonate moiety with the amino acid residues around the cofactor and the head of opposing side points to the front of F430. HS−CoB also binds to the substrate channel via salt bridges between its threoninephosphate moiety and residues near the surface of the protein matrix. These configurations of the cofactor and the coenzymes result in preservation of a hydrophobic environment of the active center during the enzymatic reaction for protection of the highly reactive Ni(I) species from bulk solvent (Fig. 3a). At the same time, the crystal structure of another inactivated state of MCR, MCR_{silent}, was resolved at a resolution of 2 Å and was found to have a generally conserved structure except for the binding of CoM−S−S−CoB to the substrate-binding channel (Fig. 3b). Both structures were later refined to 1.16 and 1.8 Å, respectively.[19]

Subsequent crystal structures were found to exhibit inactivated state containing the product or substrate analogues.[20–24] Comparing the crystal structures of MCR obtained from *M. marburgensis* with those from the phylogenetically different methanogens, such as *Methanopyrus kandleri*, *Methanosarcina barkeri*, *Methanothermococcus thermolithotrophicus*, and *Methanotorris formicicus*, revealed highly conserved structures especially in active sites while different charges are observed on the protein surfaces. In addition, most of the six post-translationally modified amino acids such as 1-*N*-methylhistidine, 5-methylarginine, 2-methylglutamine, *S*-methylcysteine, thioglycine, and didehydroaspartate are conserved in a side range of methanogens and found in the substrate-binding channel to stabilize the hydrophobic structure.[18,23] Furthermore, it has been proposed that the substrate binding to the appropriate position induces conformational changes of MCR to bring CH_3S−CoM closer to the nickel center of F430 by comparing the crystal structure of MCR containing the natural substrate HS−CoB having a heptanoyl moiety linked to the thiol group with MCR containing HS−CoB analogues having pentanoyl-, hexanoyl-, octanoyl- or nonanoyl-containing derivatives of HS–CoB.[20,21,25,26] On the other hand, crystal structure of MCR obtained from methanotrophic archaea collected from Black Sea mat catalyzing anaerobic methane oxidation was found to show the similar structure with that from methanogenic archaea.[27]

1.2 F430 cofactor

F430 was isolated as a nickel-containing cofactor in 1980.[28,29] The Ni(II) state of F430 in solution without the protein matrix is yellow and has absorption maxima at 274 nm and 430 nm, whereas the Ni(I) state is green with absorption maxima at 383 nm and 759 nm (Fig. 4a).[30,31] A pentamethylester of F430 known as F430M, has been utilized to evaluate physicochemical properties and reactivity because it is highly soluble in non-coordinating organic solvents. The structures of F430 and F430M derivatives were determined from NMR and X-ray crystal structural analyses.[32–34] F430 is a natural nickel porphyrinoid that has the most saturated tetrapyrrole framework, known as hydrocorphin. The highly saturated F430 framework is responsible for the yellow color, whereas porphyrin is purple in solution. Moreover, the ATP-dependent biosynthetic pathway of F430 has been investigated; sirohydrochlorin is known to be a precursor and is converted to F430 via nickel insertion, amidation, cyclization of the *c*-acetamide side chain with six-electron reduction, and then ATP-dependent cyclization of the *g*-propionate side chain.[35–37] In addition, McrD, a protein that interacts with MCR, is expected to transfer F430 to apo-MCR.[35,38]

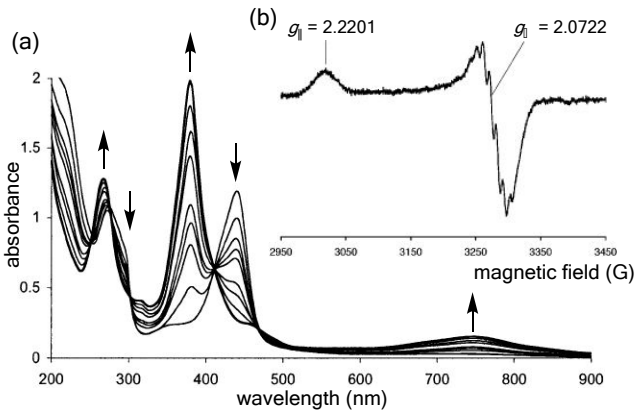

Fig. 4. Representative spectra of F430 derivatives. (a) UV-vis spectral changes of Ni(II) F430M during electrolysis to the Ni(I) state in acetonitrile. (b) X-band EPR spectrum of Ni(I) F430M generated by electrolysis in frozen acetonitrile at 130 K. Reprinted with permission from reference 31. Copyright 2003 American Chemical Society.

The nickel center of F430 is redox-active and exists in Ni(I), Ni(II), and Ni(III) oxidation states. The redox potentials of F430 derivatives for the Ni^{II}/Ni^{I} process were determined to be −0.65 V vs. NHE in an alkaline buffer solution[39] and −0.50 V for F430M in dimethylformamide (Table 1).[30] Meanwhile, the redox potential corresponding to the Ni^{III}/Ni^{II} process was determined to be +1.45 V in acetonitrile.[40] Although the redox potentials of F430 in MCR have not been determined, they are expected to be lower than those of protein-free F430.[14]

EPR spectroscopic measurements have been widely employed to evaluate the oxidation state of the nickel center in F430 derivatives, which determines EPR-active Ni(I) and Ni(III) states and the EPR-silent Ni(II) state. The Ni(I) species of F430M generated by electrochemical reduction exhibits an axial EPR spectrum ($g_{\perp}$ = 2.072 and $g_{\parallel}$ = 2.220) with superhyperfine splitting due to coupling with tetrapyrrole nitrogen atoms (Fig. 4b).[31] The Ni(I) species of F430M and native F430 obtained by chemical reduction with NaHg in tetrahydrofuran[30] and Ti(III) citrate in alkaline buffer solution, respectively, have similar EPR spectra.[39] The characteristic spectra showing $g_{\perp} < g_{\parallel}$ indicate a predominant $d_{x^2-y^2}$ configuration of the nickel center in d^9 metal complexes (S = 1/2). The Ni(III) species of F430M generated by electrochemical oxidation in acetonitrile has an axial EPR

spectrum ($g_{\perp}$ = 2.211 and $g_{\parallel}$ = 2.020), indicating that the nickel ion has a predominant d_{z^2} configuration.[40]

MCR adopts different states monitored by EPR, which depend on the environment of F430. These states include: (i) enzymatically active MCR_{red1} and MCR_{red2} with Ni(I) species, (ii) enzymatically inactive MCR_{silent} and $MCR_{ox1\text{-}silent}$ with Ni(II) species, and (iii) enzymatically inactive MCR_{ox1} with Ni(III) species and their subtypes.[14] In general, MCR_{red1} states, which are harvested under H_2 atmosphere, contain the active penta-coordinated Ni(I) species with Gln147 and are further classified into three sub-states: (i) MCR_{red1a} without coenzymes, (ii) MCR_{red1m} with CH_3S−CoM, and (iii) MCR_{red1c} with HS−CoM. These three species provide the characteristic EPR spectra of the Ni(I) state which are mostly identical with that of well-characterized Ni(I) form of F430M as shown in Fig. 4b. Slight differences in *g*-values were investigated to distinguish these three species: g_1 = 2.252; g_2 = 2.070; g_3 = 2.061 for MCR_{red1a}, g_1 = 2.252; g_2 = 2.073; g_3 = 2.064 for MCR_{red1m}, and g_1 = 2.250; g_2 = 2.071; g_3 = 2.061 for MCR_{red1c}.[14,44] The addition of HS−CoB to MCR_{red1c} induces conformational changes which bring HS−CoM closer to the nickel center. This causes partial conversion to MCR_{red2}, which represents an equilibrium state between two different species: a Ni(I) state possessing side-on coordination with the thiol group of HS−CoM and either a Ni(III) hydride complex or a nickel complex hydrogen bonded with acidic proton of the thiol group of HS−CoM.[41,42] Moreover, the MCR_{ox1} states are enzymatically inactive and estimated to be in an equilibrium state between a Ni(III) state axially ligated by thiolate of HS−CoM and a coupled Ni(II) state with a thiyl radical species.[43] MCR_{ox1} is completely transformed to MCR_{red1} upon addition of Ti(III) citrate under alkaline conditions[17] and to $MCR_{ox1\text{-}silent}$ under aerobic conditions. The latter is an inactive Ni(II) state (Fig. 3a).[18,19,44] These species are converted to MCR_{silent} under low H_2 levels in the presence of CoM–S–S–CoB (Fig. 3b).[18,19,41-44]

1.3 Reaction mechanism of MCR for methane formation

Extensive mechanistic studies have resulted in proposals of three reaction mechanisms involving different reaction intermediates including a CH_3−Ni(III) species (mechanism I) and a methyl radical species (mechanisms II and III) (Fig. 5).[12-14,45] Mechanism I (Fig. 5a) suggests that the Ni(I) species of F430 attacks the methyl group of CH_3S−CoM in a nucleophilic S_N2 reaction to form a transient CH_3−Ni(III) intermediate. Further electron transfer and hydrogen-abstraction from HS−CoM generate methane, the Ni(I) species, and disulfide product, CoM–S–S–CoB. This mechanism was proposed as a result of characterization of reactions of the F430 derivatives [46,47] and reactions of MCR_{red1}[22,48-52] with activated alkyl reagents. It was found that 2 equiv. of the Ni(I) species of F430M reacts with 1 equiv. of electrophilic methyl donors, such as methyl iodide, methyl tosylate, and trimethylsulfonium compound, to afford 1 equiv. of methane and 2 equiv. of the Ni(II) species. The CH_3−Ni(II) species of F430M was also identified as an intermediate in NMR measurements at low temperature.[46,47] Similarly, the MCR_{red1} state also reacts with methyl iodide, methyl bromide, and 3-bromopropionate to form a CH_3− or (alkyl)C−Ni(III) complex and structures were determined by X-ray structural analysis and X-ray absorption spectroscopy.[22,48-50]

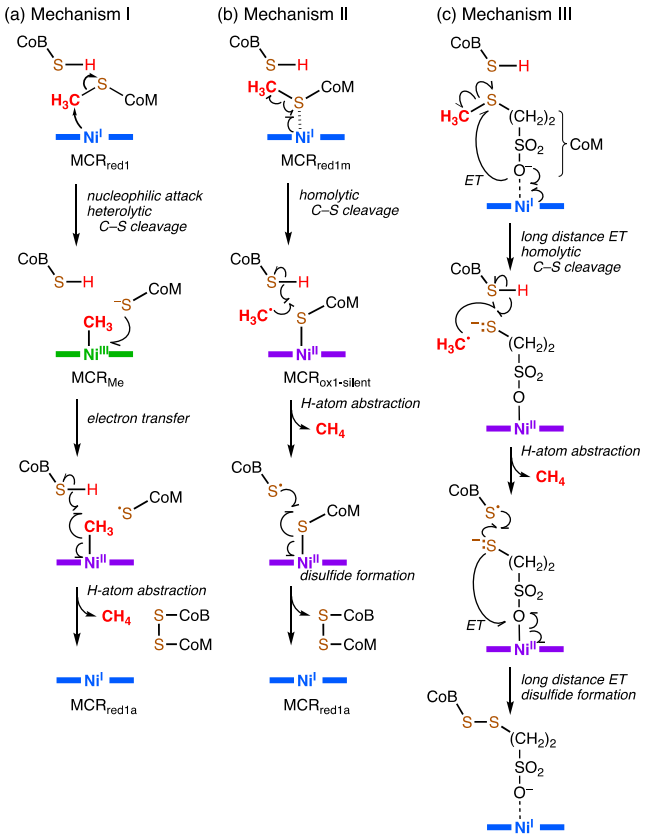

Fig. 5. Three representative reaction mechanisms for methane generation by MCR. MCR_{red1m} and $MCR_{ox1\text{-}silent}$ species are expected from EPR measurements under specific conditions.

Furthermore, the CH_3−Ni(III) complex in MCR was found to react with thiolate compounds including HS−CoM and HS−CoB to form corresponding thioether products resulting in the regeneration of the MCR_{red1} state and with Ti(III) citrate to produce methane and the MCR_{red1} state.[51,52] These results support the reaction mechanism which includes formation of a CH_3-Ni(III) intermediate. However, this intermediate has not been observed in the reaction of the MCR_{red1} state with CH_3S−CoM. Moreover, hybrid density functional theory (DFT) predicts that formation of the CH_3−Ni(III) species in a nucleophilic S_N2-type attack of the Ni(I) species on the methyl group of the thioether moiety is endergonic and not feasible due to the 21.8 kcal·mol^{-1} energy barrier.[53-56]

In contrast, mechanism II includes the homolytic cleavage of the C–S bond of CH_3S–CoM promoted by the Ni(I) species in the first step to generate a transient methyl radical intermediate. Next, hydrogen atom abstraction from HS−CoB generates methane as shown in Fig. 5b. The generated Ni(II)−thiolate complex reacts with the thiyl radical of HS−CoB to generate the Ni(II)−disulfide anion radical complex, transferring one electron to the nickel center to form the original Ni(I) species and the disulfide compound. This mechanism is supported by theoretical studies and a recent investigation on the reaction of MCR_{red1} state with substrate analogs containing thioether or thiol moieties. Hybrid DFT calculations predict that the energies required in the first and second steps in mechanism II are 15.1 and 5.9 kcal·mol^{-1}, respectively, suggesting that the first rate-

determining step is more energetically favorable relative to the analogous step in mechanism I.[53-56] Ragsdale and co-workers have recently proposed mechanism III which also includes homolysis of the C–S bond of CH_3S–CoM to generate the methyl radical species while the generated thiyl radical is reduced via a long distance electron transfer as shown in Fig. 5c. This mechanism is supported by spectroscopic, kinetic and computational studies which indicate the Ni(I)–O coordination by the sulfonate group of CH_3S–CoM.[45] Considering the distance between the sulfur atoms of the two coenzymes, this reaction mechanism appears to be reasonable.

Other reaction mechanisms initiated by oxidative addition, which form the ternary intermediate with a side-on C−S bond of CH_3S−CoM or C−H bond of methane coordinated to the nickel center, and protonation of CH_3S−CoM, which promotes the formation of the CH_3−Ni(III) intermediate, were estimated to be energetically unfavorable according to the hybrid DFT calculation.[58]

2. Model systems for MCR

2.1 Nickel complexes as a model of the F430 cofactor

In parallel with mechanistic studies using native MCR itself, methane generation activity by nickel complex-based model systems have been investigated. In terms of similarity of the tetrapyrrole framework with hydrocorphin, porphyrinoids have been employed as model complexes of F430.[59,60] A series of porphyrinoids including porphyrin and chlorin, such as nickel(II) octaethylisobacteriochlorin, Ni^{II}(OEiBC) (Fig. 6a), with a highly saturated tetrapyrrole framework have been investigated because the relatively stable Ni(I) species (Ni^{I}(OEiBC)$^-$) is quantitatively prepared by electrochemical or chemical reduction in organic solvents.[61-65] The redox potential corresponding to the Ni^{II}/Ni^{I} process was determined to be −1.28 V in acetonitrile,[61] which is significantly negative compared to those of F430 derivatives (Table 1). Ni^{I}(OEiBC)$^-$, which was prepared by electrochemical reduction or chemical reduction with Na/Hg, has an axial EPR spectrum ($g_\perp$ = 2.073 and $g_\parallel$ = 2.201) with hyperfine coupling similar to spectra of F430 derivatives.[61] Ni^{I}(OEiBC)$^-$ reacts with methyl iodide with 2:1 stoichiometry to produce Ni^{II}(OEiBC) and methane as previously observed in F430M. Furthermore, Ni^{II}(OEiBC) catalyzes reductive dehalogenation and homocoupling reactions for other alkyl halides to generate products which depend on the polarity of the organic solvent used for the reactions. Although the transient (alkyl)C−Ni(III) intermediate was not identified, the reactivity trend increases with higher leaving group ability and less steric hindrance at the reactive carbon center of the substrates. This indicates that a nucleophilic S_N2-type reaction mechanism is likely to occur as the initial step of the reaction including the rate-determining attack of the Ni(I) species on the substrates.[62-65]

On the other hand, other macrocyclic nickel complexes including azacyclam ligands have also been investigated as model complexes of F430.[66-72] For instance, nickel(II) 1,4,8,11-tetramethyl-1,4,8,11-tetraazacyclotetradecane (nickel(II) tetramethytetraazacyclodecane, Ni(tmc)$^{2+}$, Fig. 6b) has a redox potential of –0.89 V for the Ni^{II}/Ni^{I} process in alkaline aqueous solution[68] (Table 1) and electrochemically or photochemically prepared Ni(I) species (Ni(tmc)$^+$) can react with alkyl halides to afford isolable (alkyl)C−Ni(II) complexes and coupling products. The reaction is estimated to proceed in a radical-based mechanism according to the result showing high substrate reactivity accompanied by an increase of the substituent number on the carbon center and the results of a radical trapping experiment. Moreover, Tatsumi and coworkers have recently reported a series of nickel(II) tetramethytetraazacyclodecane complexes with a thioether moiety (nickel(II) 1,8-dimethyl-4,11-bis[(2-methylthio)ethyl]-1,4,8,11-tetraaza-1,4,8,11-cyclotetradecane, Ni(dmmtc)$^{2+}$) (Fig. 6c).[70-72] Crystal structures of the Ni(I) species were obtained and methane generation via intramolecular C−S bond cleavage was demonstrated.

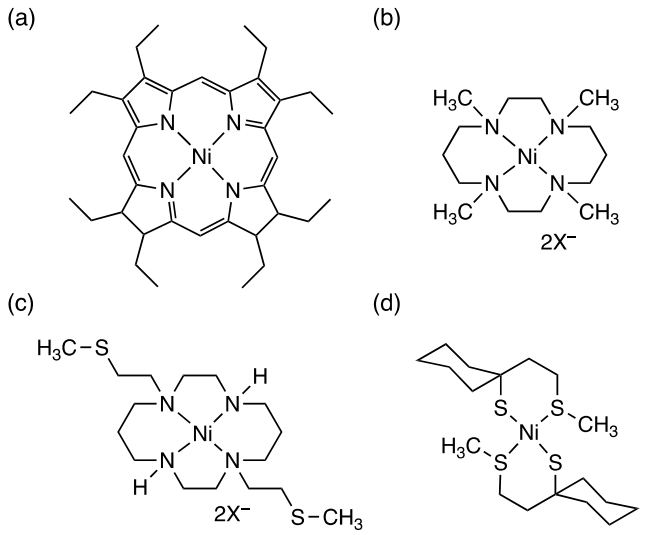

Fig. 6. Structures of nickel complexes formed in a model of F430. (a) Ni^{II}(OEiBC), (b) Ni(tmc)$^{2+}$, (c) Ni(dmmtc)$^{2+}$, (d) bis{1-[2-(methylthio)ethyl]cyclohexanethiolato}nickel(II).

Table 1. Redox potentials of nickel complexes for the Ni^{II}/Ni^{I} process.

complex	Ni^{II}/Ni^{I} (V vs. NHE)	reference
F430	−0.65[a]	39
12,13-di-epi F430	−0.62[a]	39
F430M	−0.50[b]	30
Ni(OEiBC)	−1.28[c]	61
Ni(tmc)$^{2+}$	−0.89[a]	68
5,6-DHNibs	–0.89[b]	77
Ni(TDHC)	−0.34[d]	83
	−0.25[c]	84

rMb(Ni(TDHC))	−0.45[d]	83
Ni(DDHC)	−0.41[c]	84

[a] in an alkaline buffer solution. [b] in dimethylformamide. [c] in acetonitrile (–1.52 V vs SCE). [d] in a neutral buffer solution.

The reaction mechanism, which involves activation of the C−S bond of CH_3S−CoM in a reaction with the thiyl radical of HS−CoB to form a sulfuranyl intermediate and subsequent methyl transfer to the Ni(I) species with protonation to achieve methane generation, was individually proposed by Jaun, Berkessel and Tada in the 1990s.[40,73,74] Furthermore, Jaun, Pfaltz and coworkers examined the postulated mechanism using bis{1-[2-(methylthio)ethyl]cyclohexanethiolato}nickel(II) (nickel(II) thiolate-thioether complex, (Fig. 6d)) and demonstrated methane generation and disulfide formation upon photoirradiation. This result indicated the presence of a sulfuranyl intermediate and the C−S bond cleavage. An active Ni(I) species has not been identified and the reaction mechanism is unclear.[75]

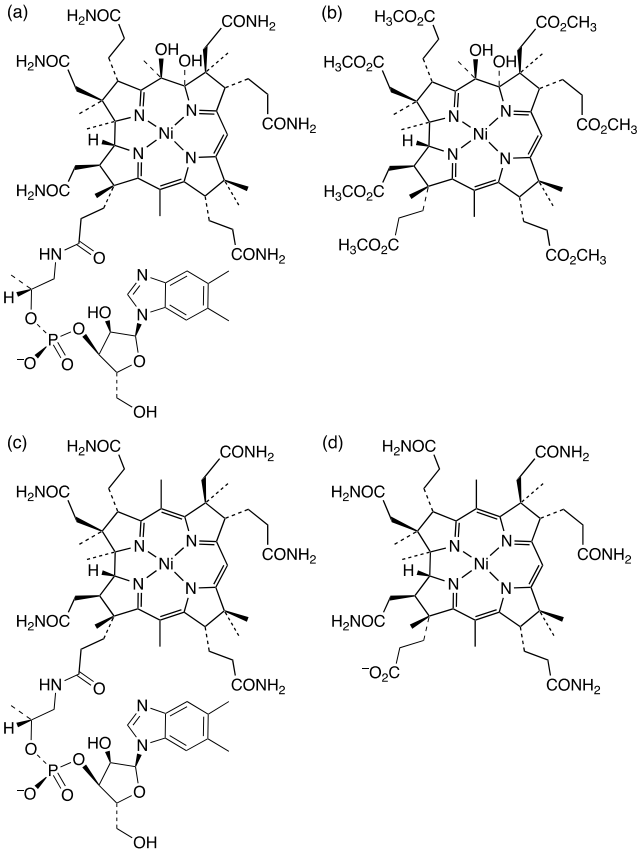

Fig. 7. Structures of nickel analogs of cobalamin, investigated as a candidate of the model of F430: (a) 5,6-DHNibl, (b) 5,6-DHNibs, (c) Nibl, (d) Niby.

2.2 Nibalamin as a new model for MCR

In addition to a series of small nickel complexes, nickel-analogs of cobalamin where the nickel ion is captured by a metal free corrinoid framework, have recently been reported. These semi-synthetic models using a monoanionic ligand are found to be structurally similar to the hydrocorphin framework. Zelder and coworkers have prepared 5,6-dihydroxy-5,6-dihydrogenonibalamins from naturally occurring cobalamin via ring-opening, demetalation/ring-closure and nickel complexation (5,6-DHNibl) (Fig. 7a).[76] UV-vis spectrum of 5,6-DHNi^{II}bl in H_2O is similar to that observed by Ni(II) species of F430 (λ_{max} = 436 nm, $\Delta\lambda_{max}$ = 1 nm). Furthermore, electrochemical and spectrochemical properties of hydrophobic 5,6-dihydroxy-heptamethyl nibyrinate (5,6-DHNibs) (Fig. 7b) were demonstrated in a model of F430M. The reversible Ni^{II}/Ni^{I} redox process was monitored and EPR signals of the Ni(I) species ($g_{\perp}$ = 1.989, $g_{\parallel}$ = 2.194 in CH_3CN at 110 K) were found to be similar to those of F430M.[77]

Kräutler and coworkers successfully inserted nickel ion into metal-free hydrogenobalamin and hydrogenobyric acid to produce nibalamin and nibyric acid, respectively (Fig. 7cd),[78] after the metal-free corrinoids were prepared in a biological process.[81] The coordination mode of Ni(II) in Ni^{II}by (Fig. 7d) is revealed by crystal structure analysis, indicating that the adaptation of the coordination geometry is comparable with that of synthetic racemic Ni(II)-corrin.[79,80] Zn and Rh-analogs of cobalamin were also constructed.[81,82]

Both nickel-analogs of cobalamin are expected to promote a reaction similar to the MCR reaction, as well as dehalogenation and/or C–C bond coupling.

2.3 Protein-based functional models of MCR

Extensive investigations of model complexes of F430 have clarified the enzymatic reaction. However, the protein matrix of MCR, which regulates and promotes the enzymatic reaction, has not been considered in designs of model systems using small metal complexes. In this context, we have established a protein-based functional model of MCR by reconstitution of an appropriate hemoprotein with a model complex of F430 to replicate the physicochemical properties and reactivity of MCR under physiological conditions and evaluated effects of the protein matrix in the enzymatic reaction (Fig. 8a).[83-85] In general, a hydrophobic heme pocket, which binds a native heme cofactor with a ligating amino acid residue in a hemoprotein, will function as an attractive coordination scaffold providing a specific environment within the protein matrix for an artificial cofactor.[86,87]

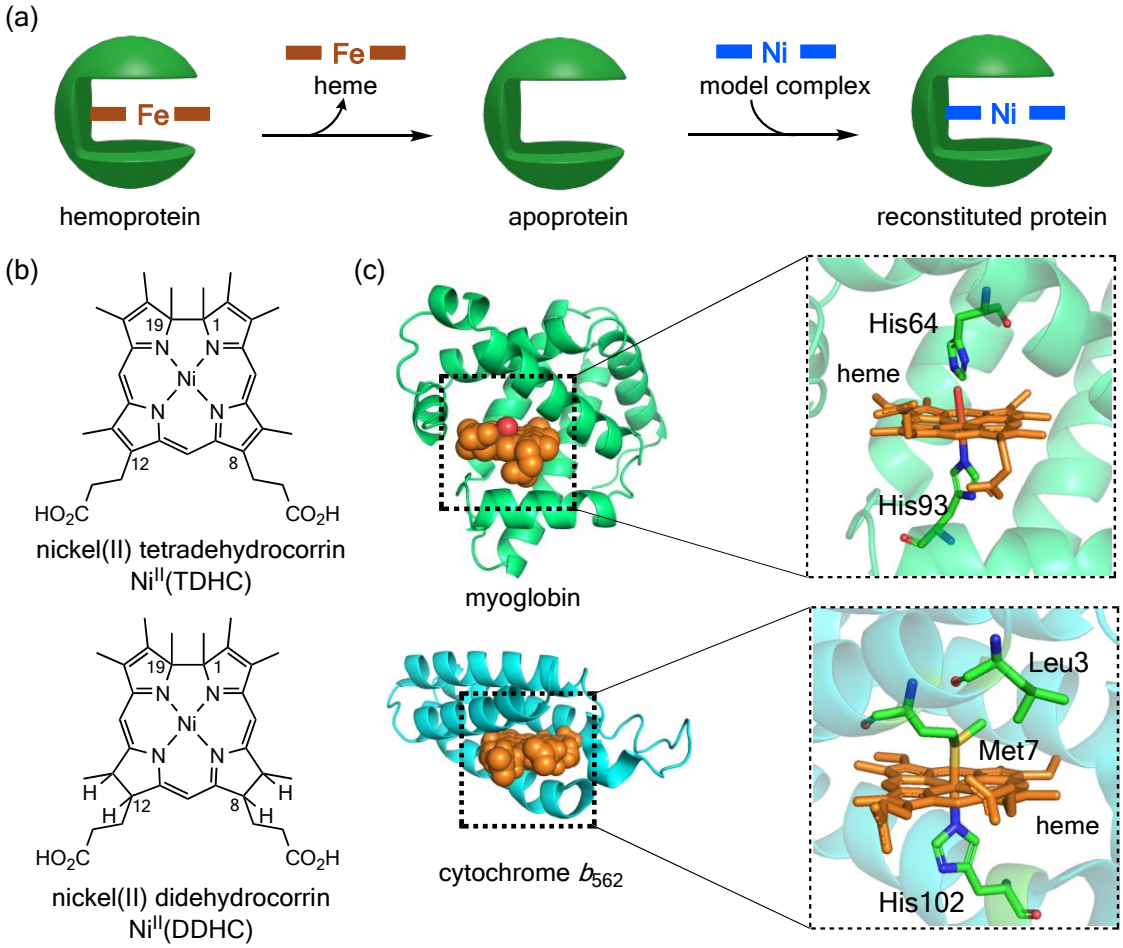

Fig. 8. (a) Schematic representation of reconstitution of hemoprotein with a model complex as an artificial cofactor. (b) Chemical structures of nickel(II) tetradehydrocorrin and nickel(II) didehydrocorrin. (c) Protein structure of myoglobin (PDB ID: 2MBW) and cytochrome b_{562} (PDB ID: 1QPU).

2.3.1 First model of MCR: myoglobin reconstituted with nickel corrinoid. Nickel(II) 8,12-dicarboxyethyl-1,2,3,7,13,17,18,19-octamethyltetradehydrocorrin (nickel(II) tetradehydrocorrin, Ni^{II}(TDHC), Fig. 8b), which has a monoanionic tetrapyrrole ligand for stabilization of a low valent metal species,[88,89] was synthesized as a model complex of F430 and found to have a redox potential for the Ni^{II}/Ni^{I} process at −0.34 V in a buffer (pH 7.0)[83] and −0.25 V in acetonitrile.[84] This complex can be reduced with dithionite as a mild reductant in a neutral buffer in contrast to F430 derivatives and previous model complexes which require a strong reductant such as Ti(III) citrate or Na/Hg (Table 1).[83] Myoglobin (Mb), an oxygen-binding hemoprotein, has a relatively stable and simple protein matrix (Fig. 8c). Addition of Ni^{I}(TDHC) into an aqueous solution of apo-form of Mb after the removal of the native heme *b* cofactor generates reconstituted myoglobin (rMb(Ni^{I}(TDHC))) as a protein-based function of model MCR. UV-vis, CD, and EPR measurements confirmed that the complex in the Ni(I) state is incorporated into a chiral environment of the protein matrix with a 1:1 ratio of the protein and Ni^{I}(TDHC) with a K_d value of 11 μM. Significant methane gas generation was observed in reactions with representative methyl donors, such as methyl iodide (37.0 nmol), methyl *p*-toluenesulfonate (2.2 nmol), and trimethylsulfonium iodide (2.0 nmol), using rMb(Ni^{I}(TDHC)) in phosphate buffer (pH 7.0 or 8.0) at 25 ºC, whereas negligible amounts of methane gas were produced by Ni^{I}(TDHC) without the protein matrix. These findings provide strongly support for a significant influence of the protein matrix in methane generation. No other gases, such as ethane, were detected. Spectroelectrochemical measurements of rMb(Ni^{I}(TDHC)) revealed a negatively shifted redox potential of Ni^{II}/Ni^{I} process at −0.45 V in neutral buffer (pH 7.0)[83] (Table 1), suggesting that the axial ligation of His93 to the nickel center in the protein matrix shifts the redox potential negatively, as shown with the TDHC cobalt complex in the myoglobin heme pocket.[88,89] However, methane generation from inert CH_3S−CoM by rMb(Ni^{I}(TDHC)) was not observed under the conventional conditions.

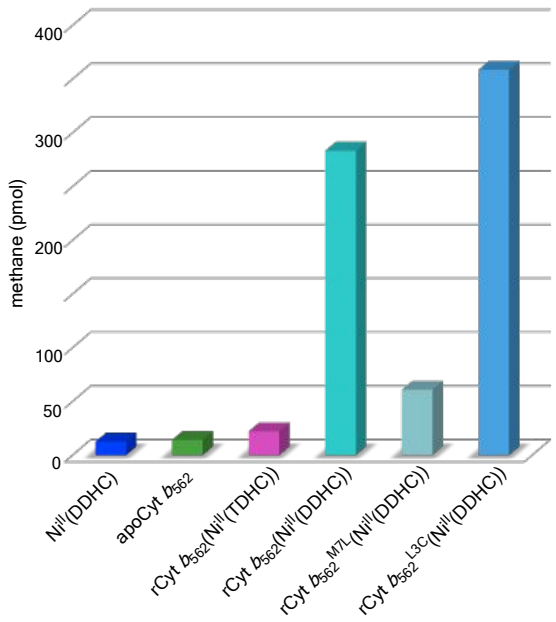

Fig. 9. Methane generation promoted by Ni^{II}(DDHC), apoCyt b_{562}, rCyt b_{562}(Ni^{II}(TDHC)), rCyt b_{562}(Ni^{II}(DDHC)), rCyt b_{562}^{M7L}(Ni^{II}(DDHC)), and rCyt b_{562}^{L3C}(Ni^{II}(DDHC)) after 2 h upon photoirradiation in the presence of [Ru(bpy)$_3$]Cl$_2$ and sodium ascorbate in 100 mM phosphate buffer (pH = 7.0) at 25 °C under an N_2 atmosphere. Total volume; 100 μL, [Ni^{II}(DDHC)] = 50 μM, [apoCyt b_{562} variant] = 150 μM.

2.3.2 Dehalogenation catalyzed by the nickel corrinoid reconstituted protein. Since methane can be generated from various activated methyl donors, rMb(Ni^{I}(TDHC)) was expected to react with alkyl halides, especially benzyl bromide derivatives. Reaction with benzyl bromide and 1-phenylethyl bromide provided reductively dehalogenated products, toluene (9.8 μM with the initial rate constant of 0.39 μM·min^{-1}) and ethylbenzene (1.0 μM with the initial rate constant of 0.057 μM·min^{-1}), without any production of homocoupling byproducts. The complex does not react with cumyl bromide.[85] This result shows that the reactivities of a series of benzyl bromide derivatives increase in the order of primary > secondary > tertiary benzylic carbons, suggesting a steric effect on the reaction with the nickel center in the initial step. Furthermore, Hammett plot studies using a series of *para*-substituted benzyl bromides indicate enhancement of reactivity with electron-withdrawing substituents showing the positive slopes (ρ > 0) with the plots of rate constants for generation of toluene derivatives against polar substituent constants. These results indicate that the reaction of the Ni(I) species to benzylic position in the initial step proceeds in the nucleophilic S_N2-type mechanism to form a transient (alkyl)C−Ni(III) species in accordance with mechanism I. In addition, an isotope-labeling mass spectrometry experiment for the dehalogenation reaction of benzyl bromide in a D_2O buffer (pD 7.0) exhibited a complete isotope shift of generated toluene, indicating that the transient (alkyl)C−Ni(III) species is rapidly protonated to afford the reductively dehalogenated product.

2.3.3 C–S Bond cleavage promoted by nickel corrinoid in cytochrome b_{562}. In contrast to inert rMb(Ni^{I}(TDHC)) for CH_3S−CoM, a different set of protein-based functional models for MCR was constructed to replicate methane generation via the C−S bond cleavage.[84] Nickel(II) 8,12-dicarboxyethyl-1,2,3,7,13,17,18,19-octamethyldidehydrocorrin (nickel(II) didiehydrocorrin, Ni^{II}(DDHC), Fig. 8b) was found to have a negatively shifted redox potential at −0.41 V in acetonitrile[84] relative to that of Ni(TDHC) because the highly saturated monoanionic tetrapyrrole ligand is expected to impart higher reactivity to the Ni(I) species (Table 1). Furthermore, cytochrome b_{562} (Cyt b_{562}), a hemoprotein responsible for electron transfer with a hexa-coordinated heme *b* cofactor with axial ligation with His102 and Met7, has attracted attention as a new protein matrix (Fig. 8c). The proximity effect between the metal center and the thioether moiety of Met7 was expected to promote C−S bond cleavage followed by methane generation. The addition of Ni^{II}(DDHC) to an aqueous solution of the apo-form of Cyt b_{562} afforded reconstituted Cyt b_{562} (rCyt b_{562}(Ni^{II}(DDHC))). Next, rCyt b_{562}(Ni^{II}(DDHC)) was reduced to obtain the Ni(I) species upon photo-irradiation in the presence of tris(2,2'-bipyridine)ruthenium(II) chloride and sodium ascorbate as a photosensitizer and a sacrificial reagent, respectively. A mass spectroscopy study indicated that the formation of part of the demethylated apoCyt b_{562}, which lost one methyl group, and further methane generation could be detected by GC analysis. Employment of rCyt b_{562}^{M7L}(Ni^{II}(DDHC)) where Met7 was replaced with Leu7 in an investigation of the role of Met7, showed significantly decreased methane generation and the demethylated protein was not detected in mass spectral analysis after the reaction. These results indicate the possibility that methane is derived from the Met7 C−S bond cleavage promoted by the Ni(I) species in the heme pocket. Furthermore, rCyt b_{562}^{L3C}(Ni^{II}(DDHC)), where Cys was introduced instead of Leu3 in the vicinity of Met7, was investigated, because Met7 and Cys3, which are close to the active Ni(I) species appear to provide structural features of CH_3S−CoM, and HS−CoB, respectively. The result of methane generation shown in Fig. 9 indicates that cysteine substitution enhances the yield by 24% compared to rCyt b_{562}(Ni^{II}(DDHC)). These results clearly show the significance of precise arrangements of the thioether, the thiol, and the nickel center in the protein matrix for the enzymatic reaction via the C−S bond cleavage of the inert CH_3–S moiety.

Taken together, our protein-based functional models for MCR show similar physicochemical properties and reactivity and generate methane as a product from model substrates. The hydrophobic cavity of hemoprotein can provide an effective platform not only for the binding site of the active nickel complex but also for replication of the appropriate second coordination sphere.

Summary and outlook

Since methane is recognized as an attractive energy source as well as a potent greenhouse gas, investigations of MCR in context of biological methane formation and degradation is important. Although MCR was discovered in methanogens in the 1970s, studies focusing on the structure and function of MCR have been quite challenging because of the high oxygen-

sensitivity of the active species of MCR. After purification of MCR was established in the 1990s, wide-ranging intensive studies have been carried out including elucidation of crystal structures and determination of detailed states of MCR by spectroscopic measurements, such as UV-vis absorption spectroscopy, MCD, and EPR. Furthermore, recent efforts have led to the proposal that MCR is an essential enzyme for biological anaerobic oxidation of short chain alkanes including methane, ethane, and butane in methanotrophs. Two types of the representative reaction mechanisms have been proposed and are well recognized in this field including formation of a transient CH_3−Ni(III) intermediate or methyl radical species. The former is based on the reaction of MCR_{red1} with activated model substrates and F430 model complexes, whereas the latter is supported by theoretical studies and recent experimental evidence based on the reaction of MCR_{red1} with inert model substrates and currently appears to be the most acceptable mechanism for MCR. Although these proposals are predominantly based on spectroscopic analyses, definitive evidence including crystal structures of MCR with the active state and reaction intermediate will reveal the reaction mechanism of MCR. Furthermore, protein-based functional models containing model complexes of the F430 cofactor are useful in characterizing the mechanism of the methane generation because they can be more reliably manipulated relative to the inherently labile enzyme itself. In particular, artificially-modified proteins with an active metal complex have great potential to provide insights into understanding the reaction mechanism of a complicated enzyme as well as developing new artificial metalloenzymes. Recently progress using hemoproteins reconstituted with nickel cofactor models is expected to advance the research area of nickel complex chemistry within a protein matrix and result in construction of efficient methane generation and oxidation systems.

Conflicts of interest

There are no conflicts to declare.

Acknowledgements

This work was financially supported by Grants-in-Aid for Scientific Research provided by JSPS KAKENHI Grant Numbers JP15H05804, JP16H06045, JP17J00008, JP18KK0156, JP18K19099, and JP20H0043. K.O. appreciates support from JST PRESTO (JPMJPR15S2) and SICORP. Y.M. appreciates support from the JSPS Research Fellowship for Young Scientists.

Notes and references

1 P. Turano and Y. Lu, in *Handbook on Metalloproteins*, eds. I Bertini, A. Sigel and H. Sigel, Marcel Dekker, New York, 2001, pp. 269–356.
2 W. Kaim, B. Schwederski and A Klein, in *Bioinorganic Chemistry*, Chichester, 2013, pp. 57–76.
3 B. Kräutler, in *Advances in Bioorganometallic Chemistry*, eds. T. Hirao and T. Moriuchi, Elsevier, Amsterdam, 2019, pp. 399–430.
4 R. P. Gunsalus and R. S. Wolfe, *FEMS Microbiol. Lett.* 1978, **3**, 191–193.
5 A. Eschenmoser, *Ann. NY Acad. Sci.*, 1986, **471**, 108–129.
6 R. K. Thauer, A. K. Kaster, H. Seedorf, W. Buckel and R. Hedderich, *Nat. Rev. Microbiol.*, 2008, **6**, 579−591.
7 P. N. Evans, J. A. Boyd, A. O. Leu, B. J. Woodcroft, D. H. Parks, P. Hugenholtz and G. W. Tyson, *Nat. Rev. Microbiol.,* 2019, **17**, 219−232.
8 M. Krüger, A. Meyerdierks, F. O. Glöckner, R. Amann, F. Widdel, M. Kube, R. Reinhardt, R. Kahnt, R. Böcher, R. K. Thauer and S. Shima, *Nature,* 2003, **426**, 878−881.
9 S. Scheller, M. Goenrich, R. Boecher, R. K. Thauer and B. Jaun, *Nature,* 2010, **465**, 606−608.
10 R. Laso-Pérez, G. Wegener, K. Knittel, F. Widdel, K. J. Harding, V. Krukenberg, D. V. Meier, M. Richter, H. E. Tegetmeyer, D. Riedel, H.-H. Richnow, L. Adrian, T. Reemtsma, O. J. Lechtenfeld and F. Musat, *Nature,* 2016, **539**, 396−401.
11 S.-C. Chen, N. Musat, O. J. Lechtenfeld, H. Paschke, M. Schmidt, N. Said, D. Popp, F. Calabrese, H. Stryhanyuk, U. Jaekel, Y.-G. Zhu, S. B. Joye, H. H.-H. Richnow, F. Widdel and F. Musat, *Nature,* 2019, **568**, 108−111.
12 U. Ermler, *Dalton Trans.,* 2005, 3451−3458.
13 S. W. Ragsdale, S. Raugei, B. Ginovska and T. Wongnate, in *The Biological Chemistry of Nickel*, eds. D. Zamble, M. Rowińska-Żyrek and H. Kozlowski, Royal Society of Chemistry, Cambridge, UK, 2017, pp 149–169.
14 R. K. Thauer, *Biochemistry,* 2019, **58**, 5198−5220.
15 R. P. Gunsalus and R. S. Wolfe, *J. Biol. Chem.,* 1980, **255**, 1891−1895.
16 S. Rospert, R. Bocher, S. P. J. Albracht and R. K. Thauer, *FEBS Lett.,* 1991, **291**, 371– 375.
17 M. Goubeaud, G. Schreiner and R. K. Thauer, *Eur. J. Biochem.,* 1997, **243**, 110−114.
18 U. Ermler, W. Grabarse, S. Shima, M. Goubeaud and R. K. Thauer, *Science,* 1997, **278**, 1457−1462.
19 W. Grabarse, F. Mahlert, E. C. Duin, M. Goubeaud, S. Shima, R. K. Thauer, V. Lamzin and U. Ermler, *J. Mol. Biol.,* 2001, **309**, 315−330.
20 W. G. Grabarse, F. Mahlert, S. Shima, R. K. Thauer and U. Ermler, *J. Mol. Biol.,* 2000, **303**, 329−344.
21 P. E. Cedervall, M. Dey, A. R. Pearson, S. W. Ragsdale and C. M. Wilmot, *Biochemistry,* 2010, **49**, 7683−7693.
22 P. E. Cedervall, M. Dey, X. Li, R. Sarangi, B. Hedman, S. W. Ragsdale and C. M. Wilmot, *J. Am. Chem. Soc.,* 2011, **133**, 5626−5628.
23 T. Wagner, J. Kahnt, U. Ermler and S. Shima, *Angew. Chem. Int. Ed.,* 2016, **55**, 10630–10633.
24 T. Wagner, C. E. Wegner, J. Kahnt, U. Ermler and S. Shima, *J. Bacteriol.,* 2017, **199**, 199:e00197-17.
25 S. Ebner, B. Jaun, M. Goenrich, R. K. Thauer and J. Harmer, *J. Am. Chem. Soc.,* 2010, **132**, 567−575.
26 T. Wongnate and S. W. Ragsdale, *J. Biol. Chem.,* 2015, **290**, 9322–9334.
27 S. Shima, M. Krueger, T. Weinert, U. Demmer, J. Kahnt, R. K. Thauer and U. Ermler, *Nature,* 2012, **481**, 98−101.
28 W. B. Whitman and R. S. Wolfe, *Biochem. Biophys. Res. Commun.,* 1980, **92**, 1196−1201.
29 G. Diekert, B. Klee and R. K. Thauer, *Arc. Microbiol.,* 1980, **124**, 103−106.
30 B. Jaun and A. Pfaltz, *J. Chem. Soc., Chem. Commun.,* 1986, 1327−1329.
31 R. Piskorski and B. Jaun, *J. Am. Chem. Soc.,* 2003, **125**, 13120−13125.
32 A. Pfaltz, B. Jaun, A. Fassler, A. Eschenmoser, R. Jaenchen, H. H. Gilles, G. Diekert and R. K. Thauer, *Helv. Chim. Acta,* 1982, **65**, 828−865.
33 H. Won, M. F. Summers, K. D. Olson and R. S. Wolfe, *J. Am. Chem. Soc.,* 1990, **112**, 2178−2184.
34 G. Färber, W. Keller, C. Kratky, B. Jaun, A. Pfaltz, C. Spinner, A. Kobelt and A. Eschenmoser, *Helv. Chim. Acta,* 1991, **74**, 697−716.
35 K. Zheng, P. D. Ngo, V. L. Owens, X.-p. Yang and S. O. Mansoorabadi, *Science*, 2016, **354**, 339–342.
36 S. J. Moore, S. T. Sowa, C. Schuchardt, E. Deery, A. D. Lawrence, J. V. Ramos, S. Billig, C. Birkemeyer, P. T. Chivers, M. J. Howard, S. E. J. Rigby, G. Layer and M. J. Warren, *Nature*, 2017, **543**, 78–82.
37 S. M. Ghebreamlak, S. O. Mansoorabadi, *ChemBioChem*, 2020, **21**, 1723–1728.
38 S. O. Mansoorabadi, K. Zheng, P. D. Ngo, in *Encyclopedia of Inorganic and Bioinorganic Chemistry*, 2017, John Wiley & Sons, eibc2488.
39 C. Holliger, A. J. Pierik, E. J. Reijerse and W. R. Hagen, *J. Am. Chem. Soc.*, 1993, **115**, 5651−5656.
40 B. Jaun, *Helv. Chim. Acta,* 1990, **73**, 2209−2217.

41 S. P. J. Albracht, D. Ankel-Fuchs, R. Bocher, J. Ellermann, J. Moll, J. W. Vanderzwaan and R. K. Thauer, *Biochim. Biophys. Acta,* 1988, **955**, 86−102.
42 F. Mahlert, W. Grabarse, J. Kahnt, R. K. Thauer and E. C. Duin, *J. Biol. Inorg. Chem.,* 2002, **7**, 101−112.
43 E. C. Duin, L. Signor, R. Piskorski, F. Mahlert, M. D. Clay, M. Goenrich, R. K. Thauer, B. Jaun and M. K. Johnson, *J. Biol. Inorg. Chem.,* 2004, **9**, 563−576.
44 F. Mahlert, C. Bauer, B. Jaun, R. K. Thauer and E. C. Duin, *J. Biol. Inorg. Chem.,* 2002, **7**, 500−513.
45 A. Patwardhan, R. Sarangi, B. Ginovska, S. Raugei and S. W. Ragsdale, *J. Am. Chem. Soc*., 2021, **143**, 5481–5496.
46 B. Jaun and A. Pfaltz, *J. Chem. Soc., Chem. Commun.,* 1988, 293−294.
47 S.-K. Lin and B. Jaun, *Helv. Chim. Acta,* 1991, **74**, 1725−1738.
48 M. Dey, R. C. Kunz, D. M. Lyons and S. W. Ragsdale, *Biochemistry,* 2007, **46**, 11969–11978.
49 N. Yang, M. Reiher, M. Wang, J. Harmer and E. C. Duin, *J. Am. Chem. Soc.,* 2007, **129**, 11028–11029.
50 R. Sarangi, M. Dey and S. W. Ragsdale, *Biochemistry,* 2009, **48**, 3146–3156.
51 M. Dey, J. Telser, R. C. Kunz, N. S. Lees, S. W. Ragsdale and B. M. Hoffman, *J. Am. Chem. Soc.,* 2007, **129**, 11030−11032.
52 R. C. Kunz, M. Dey and S. W. Ragsdale, *Biochemistry,* 2008, **47**, 2661−2667.
53 V. Pelmenschikov, M. R. A. Blomberg, P. E. M. Siegbahn and R. H. Crabtree, *J. Am. Chem. Soc.,* 2002, **124**, 4039−4049.
54 V. Pelmenschikov and P. E. M. Siegbahn, *J. Biol. Inorg. Chem.,* 2003, **8**, 653−662.
55 S.-L. Chen, V. Pelmenschikov, M. R. A. Blomberg and P. E. M. Siegbahn, *J. Am. Chem. Soc.,* 2009, **131**, 9912−9913.
56 S.-L. Chen, M. R. A. Blomberg and P. E. M. Siegbahn, *Chem. Eur. J.,* 2012, **18**, 6309−6315.
57 T. Wongnate, D. Sliwa, B. Ginovska, D. Smith, M. W. Wolf, N. Lehnert, S. Raugei and S. W. Ragsdale, *Science,* 2016, **352**, 953−958.
58 S.-L. Chen, M. R. A. Blomberg and P. E. M. Siegbahn, *Phys. Chem. Chem. Phys.,* 2014, **16**, 14029−14035.
59 A. M. Stolzenberg and M. T. Stershic, *J. Am. Chem. Soc.,* 1988, **110**, 6391−6402.
60 M. W. Renner, L. R. Furenlid, K. M. Barkigia, A. Forman, H. K. Shim, D. J. Simpson, K. M. Smith and J. Fajer, *J. Am. Chem. Soc.,* 1991, **113**, 6891−6898.
61 A. M. Stolzenberg and M. T. Stershic, *Inorg. Chem.,* 1987, **26**, 3082−3083.
62 A. M. Stolzenberg and M. T. Stershic, *J. Am. Chem. Soc.,* 1988, **110**, 5397−5403.
63 G. K. Lahiri, L. J. Schussel and A. M. Stolzenberg, *Inorg. Chem.,* 1992, **31**, 4991−5000.
64 G. K. Lahiri and A. M. Stolzenberg, *Inorg. Chem.,* 1993, **32**, 4409−4413.
65 M. C. Helvenston and C. E. Castro, *J. Am. Chem. Soc.,* 1992, **114**, 8490−8496.
66 M. J. D'Aniello and E. K. Barefield, *J. Am. Chem. Soc.,* 1976, **98**, 1610−1611.
67 A. Bakac and J. H. Espenson, *J. Am. Chem. Soc.,* 1986, **108**, 713−719.
68 M. S. Ram, A. Bakac and J. H. Espenson, *Inorg. Chem.,* 1986, **25**, 3267−3272.
69 A. Bakac and J. H. Espenson, *J. Am. Chem. Soc.,* 1986, **108**, 719−723.
70 J. Nishigaki, T. Matsumoto and K. Tatsumi*, Eur. J. Inorg. Chem.,* 2010, 5011−5017.
71 J. Nishigaki, T. Matsumoto and K. Tatsumi, *Inorg. Chem.,* 2012, **51**, 3690−3697.
72 J. Nishigaki, T. Matsumoto and K. Tatsumi, *Inorg. Chem.,* 2012, **51**, 5173−5187.
73 A. Berkessel, *Bioorg. Chem.,* 1991, **19**, 101−115.
74 M. Tada and Y. Masuzawa, *Chem. Commun*. 1997, 2161–2162.
75 L. Signor, C. Knuppe, R. Hug, B. Schweizer, A. Pfaltz and B. Jaun, *Chem. Eur. J.,* 2000, **6**, 3508−3516.
76 C. Brenig, L. Prieto, R. Oetterli and F. Zelder, *Angew. Chem. Int. Ed.,* 2018, **57**, 16308−16312.
77 C. Brenig, L. Mosberger, O. Blacque, R. Kissner and F. Zelder, *Chem. Commun*. 2021, **57**, 7260–7263.
78 C. Kieninger, K. Wurst, M. Podewitz, M. Stanley, E. Deery, A. D. Lawrence, K. R. Liedl, M. J. Warren and B. Kräutler, *Angew. Chem. Int. Ed*., 2020, **59**, 20129–20136.
79 E. Bertele, H. Boos, J. D. Dunitz, F. Elsinger, A. Eschenmoser, I. Felner, H. P. Gribi, H. Gschwend, E. F. Meyer, M. Pesaro and R. Scheffold, *Angew. Chem. Int. Ed. Engl*., 1964, **3**, 490–496.
80 E. Bertele, R. Scheffold, H. Gschwend, M. Pesaro, A. Fischli, M. Roth, J. Schossig and A. Eschenmoser, *Helv. Chim. Acta*, 2015, **87**, 1755–
81 F. J. Widner, A. D. Lawrence, E. Deery, D. Heldt, S. Frank, K. Gruber, K. Wurst, M. J. Warren and B. Kräutler, *Angew. Chem. Int. Ed*., 2016, **55**, 11281–11286.
82 C. Kieninger, J. A. Baker, M. Podewitz, K. Wurst, S. Jockusch, A. D. Lawrence, E. Deery, K. Gruber, K. R. Liedl, M. J. Warren and B. Kräutler, *Angew. Chem. Int. Ed*., 2019, **58**, 14568–14572.
83 K. Oohora, Y. Miyazaki and T. Hayashi, *Angew. Chem. Int. Ed.,* 2019, **58**, 13813–13817.
84 Y. Miyazaki, K. Oohora and T. Hayashi, *J. Organomet. Chem.,* 2019, **901**, 120945.
85 Y. Miyazaki, K. Oohora and T. Hayashi, *Inorg. Chem.,* 2020, **59**, 11995–12004.
86 K. Oohora, A. Onoda and T. Hayashi, *Acc. Chem. Res.,* 2019, **52**, 945−954.
87 K. Oohora and T. Hayashi, *Dalton Trans*., 2021, **50**, 1940–1949.
88 T. Hayashi, Y. Morita, E. Mizohata, K. Oohora, J. Ohbayashi, T. Inoue and Y. Hisaeda, *Chem. Commun.,* 2014, **50**, 12560–12563.
89 Y. Morita, K. Oohora, A. Sawada, T. Kamachi, K. Yoshizawa and T. Hayashi, *Inorg. Chem.,* 2017, **56**, 1950–1955.